JOURNAL OF GEOPHYSICAL RESEARCH, VOL. 100, NO. A3, PAGES 3531–3537, MARCH 1, 1995

ULF pulsations in a magnetospheric waveguide: Comparison of real and simulated satellite data

Graham J. Rickard and Andrew N. Wright

Department of Mathematical and Computational Sciences, University of St. Andrews, St. Andrews, Fife, Scotland

Abstract. The representation of the Earth's magnetosphere as an MHD waveguide has prompted much recent speculation. In particular, the signatures associated with ULF pulsations sit well within the waveguide concept. We further explore the appositeness of the waveguide model by simulating data that a spacecraft would see when passing through a stimulated magnetospheric waveguide and by comparing the results with those obtained from a real spacecraft. We find that the waveguide results again compare favorably and can explain many features seen in the data. We also find that the magnetometer signature of the fast mode in a waveguide (unlike a cavity) does not have a regular oscillatory nature with constant period over a range of L shells.

1. Introduction

Recently, *Samson et al.* [1992] suggested that the dawn and dusk flanks of the magnetosphere may be better described as a waveguide, rather than a cavity. Subsequently, the waveguide model has been investigated theoretically [*Harrold and Samson,* 1992] and observationally [*Walker et al.,* 1992]. A more recent study by *Rickard and Wright* [1994] (hereinafter referred to as RW) extended waveguide modeling by generating two-dimensional (2-D) time-dependent solutions in an inhomogeneous waveguide. There it was shown that the robustness of the natural frequencies associated with ULF pulsations could be explained within the waveguide context. In particular, it was established that an Alfvén resonance associated with the $k_y \approx 0$ fast waveguide modes evolved with little sensitivity on the initial conditions (where the direction y is along the waveguide).

The numerical simulations presented in RW were also used to test the analysis given by *Wright* [1994], which provided a theoretical framework for understanding the dispersion of the fast waveguide modes and their resonant coupling to Alfvén waves. Although the work by *Wright* [1994] relied on a certain amount of approximation using WKB analysis, remarkably good agreement was obtained with the numerical results presented in RW.

While it is satisfying to have obtained a physical interpretation for the signatures of ULF pulsations, and to have this backed up by theoretical considerations, the comparison with real satellite data remains open. For example, it is commonly presumed that an almost monochromatic cavity or waveguide mode excites discrete pulsations. However, there is little evidence in certain satellite magnetometer data sets that they exist (W. J. Hughes, private communication, 1993; M. J. Engebretson, private communication, 1994). Moreover, M. J. Engebretson finds little evidence for spatially localised ULF pulsations, despite the ease with which they are observed in ground-based radar data [*Walker et al.,* 1992]. It is the gap between theory and observation that we wish to bridge in this paper. In doing so, we have to ask what are the significant features seen in the data that need explaining. The numerical simulations are necessarily limited in the parameter range that can be modeled; we do not pretend that "realistic" magnetospheric conditions can be met. It is therefore necessary to focus on important features in the data and then argue that the simulation results exhibit generic features of ULF pulsations in magnetospheric waveguides.

The layout of the paper is as follows. In section 2 we detail the specific data that we focus on. The data then motivate the simulations. The numerical methods are presented in section 3, followed by the simulation results in section 4. We then finish with a discussion and the conclusions.

Paper number 94JA02935.
0148-0227/95/94JA-02935$05.00

2. Observational Data

ULF pulsations have formed the basis of many observational studies, both from ground-based sites and from in situ measurements by satellites. For the purpose of this study we decided to focus on a specific set of data, namely that of *Lin et al.* [1992]. Pulsations, thought to be excited by the solar wind as suggested by ground observations, were diagnosed by the spacecraft DE 1 with a trajectory that took it across L shells ranging from $L \sim 13$ to $L \sim 4$.

The data set of most relevance to us is Figure 3b of *Lin et al.* [1992], here reproduced as Figure 1. It shows the three orthogonal magnetic field components observed by the satellite along its trajectory. We note that in our coordinate system (see later) we have the magnetic field components (b_x, b_y, b_z) which correspond to *Lin et al.*'s (b_ν, b_ϕ, b_μ) in Figure 1. The magnetic pulsations are most clearly represented in the b_ϕ data between 1630 UT and 1820 UT as four wave packets, with the wave periods clearly decreasing as the spacecraft descended through the L shells from ~400 s at 1630 UT to ~150 s at 1820 UT.

The precursors to the pulsations are thought to be represented in the b_ν and b_μ components at earlier times. In particular *Lin et al.* [1992] note that before 1715 UT, b_μ contained compressional oscillations of a decaying amplitude and with nonconstant periods (ranging from ~700 s at $L \sim 13.3$ to ~450 s at $L \sim 7.5$). They also note a 110 s poloidal wave associated with b_ν before 1620 UT.

In their summary, *Lin et al.* [1992] put together a plausible scenario for the observations. Magnetic shells in the magnetosphere resonate at their natural frequencies as a result of solar wind variations. As L decreases,

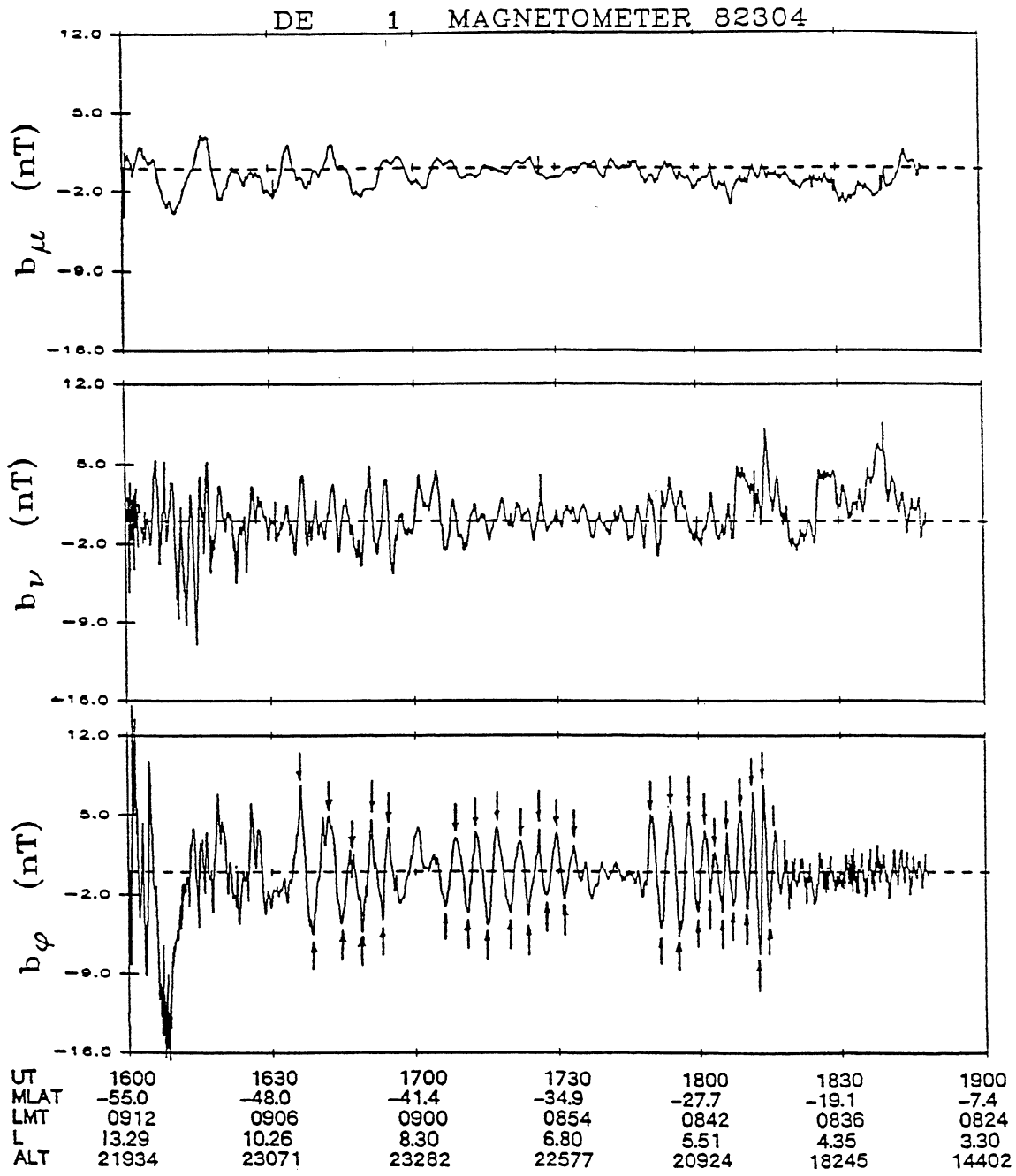

Figure 1. Magnetic field data taken from the spacecraft DE 1 (reproduced by kind permission from Figure 3b of *Lin et al.* [1992]).

so do the azimuthal field line oscillation periods with the period changes occurring on "closely adjacent field lines." Furthermore, decaying compressional waves are seen in the outer magnetosphere before the onset of toroidal oscillations. *Lin et al.* [1992, p.14,874] conclude that "compressional waves might have coupled with the transverse oscillations, transferring the energy to the resonating field lines". It is this particular scenario that we wish to explore with our numerical model of a waveguide magnetosphere. As we noted earlier it is not the actual numbers we wish to reproduce, rather it is the generic features highlighted by *Lin et al.* [1992].

3. Numerical Model

The hydromagnetic box model of *Kivelson and Southwood* [1986] forms the basis of our magnetospheric waveguide. It has a uniform magnetic field $\mathbf{B} = B\hat{\mathbf{z}}$, $\hat{\mathbf{x}}$ represents the radial direction, and $\hat{\mathbf{y}}$ is a coordinate around the Earth. Infinite length in y allows us to model a waveguide rather than a cavity. The (x, y) coordinates are then the distances across the waveguide and around the flanks and on into the magnetotail, respectively (see Figure 2). The density ρ is solely a function of x. Our dimensionless units are obtained by normalizing magnetic fields by B, density by $\rho(x)$ at $x = 0$, and length by the width of the waveguide x_m, say. Our characteristic speed is the Alfvén speed at $x = 0$ ($V(x = 0)$), with the corresponding characteristic time being $x_m/V(x = 0)$. From now on we shall refer to variables in terms of these dimensionless units.

We retain exactly the same geometry as in RW and restrict our attention to a single Fourier mode in z, so that all dependent variables are functions of x, y, and time t only. The wavenumber in z (k_z) is taken to be real, so our model ionosphere is perfectly reflecting. In reality, the ionosphere will dissipate pulsations. For high Pedersen conductivities, damping may be small over a wave period, and our model should approximate this situation well for t less than the decay timescale. We solve for the velocities u_x and u_y, and the three perturbed components of the magnetic field b_x, b_y, and b_z. Perfectly reflecting conditions are used at each end in x, apart from very early times where we consider external driving on the outer boundary (see later). Symmetry conditions at $y = 0$ along the Sun-Earth line are used, while, as before, the other y boundary is taken to be open.

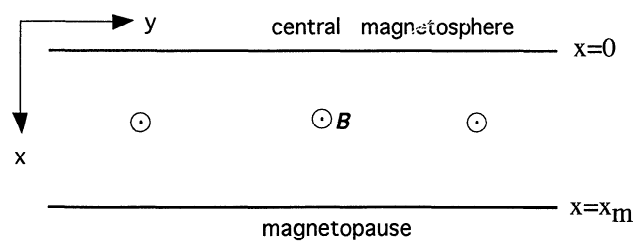

Figure 2. Geometry of the magnetospheric waveguide.

The method for numerical solution of the linearized cold MHD equations is given in RW. Suffice to say, the algorithm is second-order accurate in both space and time. As before, we use different (constant) grid spacings in x and y. The shortest spatial structure that will ultimately develop is as a result of phase mixing in the x direction, hence the use of a finer grid in x. To enable us to run waveguide simulations, we start on a not too large grid in y and run until a "significant" wave amplitude has reached the end of this box (typically $\sim 10^{-4}$ relative to our normalized system of order 1). The run is stopped, and a new section of grid in y is added on. In this way we model a waveguide accurately (but perhaps not overly efficiently). We monitor the energy and the magnetic field divergence throughout to ensure that they are significantly well conserved. Outgoing wave boundary conditions were investigated (see for example, *Vanajakshi et al.* [1989] and *Hu and Wu* [1984]), but these all produced significant ($\gtrsim 10\%$) reflection, and were not employed.

Two significant changes have been made to the model in RW. The first relates to the density profile $\rho(x)$. In RW the profile was chosen to allow only a single resonance in the domain so we could focus in detail on the fast mode dispersion and its coupling to Alfvén waves. Here however, we wish to examine data that contain many field line resonances; to that end, it is necessary to steepen the profile to allow two possible field line resonances. We favor a linear Alfvén speed profile over most of the domain since this yields a uniform phase-mixing length. However, steepening a linear profile to accommodate two resonances results in very small density scale lengths at $x = 1$. To avoid resolution problems here, we flatten $\rho(x)$ by fitting a quadratic profile for $\rho(x)$ above a critical value x_c, say, as shown in Figure 3. The solid line in Figure 3 is our resultant density profile, the dashed vertical line marks x_c, and the remaining dashed line is the original unflattened density profile with its diminishing scale length close to $x = 1$. The quadratic fit we have chosen gives us continuity of $\rho(x)$ up to the first derivative with respect to x at $x = x_c$, while giving us zero gradient of $\rho(x)$ at $x = 1$. We now need only resolve the density scale length at x_c

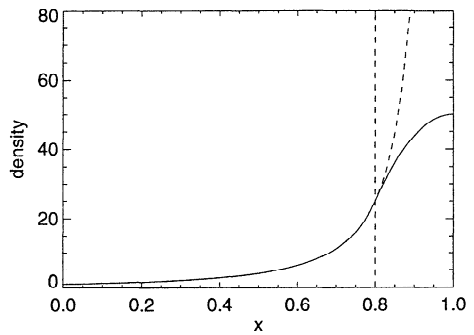

Figure 3. Density profiles $\rho(x)$ across the waveguide. The vertical dashed line marks x_c (see text), the solid line is the actual $\rho(x)$ used in the simulations, while the remaining dashed line is the $\rho(x)$ that would have been used above x_c without any smoothing.

rather then $x = 1$. This flattening impacts only very weakly on the wave propagation and coupling, while significantly easing spatial resolution and run times.

The second change from RW is in the initial conditions. In RW we assumed that a perturbation was already present in the waveguide. We made no effort to detail its origin. Here however, we take a step closer to reality by imposing a displacement ξ_x to the outer boundary at $x = 1$ for a fixed time τ, say, over a fixed length in y. Over this time interval we imagine the boundary being pushed in a certain distance, then being returned to its original position by $t = \tau$. Thereafter, the boundary conditions revert to those in RW (namely, perfectly reflecting). These conditions are intended to mimic external disturbances such as solar wind pressure pulses buffeting the outer boundary (the magnetopause). This extra condition involves relatively minor code modifications and consumes little computing time. Furthermore, the presence of resonances in our results does demonstrate that such driving conditions could indeed be a source of ULF pulsations.

Finally, we have to include our own "satellite." It travels along a specified trajectory from our outer boundary at $x = 1$ toward $x = 0$ traversing ever-reducing natural field line frequencies in the same way that DE 1 did. Time histories of all the dependent variables sampled by the satellite along its flight path then produce data in the vein of Figure 1. At any specified instant the satellite position is known, and the dependent variables at the satellite are obtained from the numerical grid by linear interpolation. The sampling rate is set high enough to resolve the highest anticipated frequencies. The satellite can be dispatched at various times and positions across the domain in order to see how a single event involving waveguide dispersion and resonance growth manifests itself in the data.

4. Results

A critical scale in the simulations is determined by the phase-mixing length $L_{ph}(x,t)$, say, at position x and time t, where $L_{ph}(x,t) = 2\pi/(\omega'_A t)$. Here $\omega'_A = d\omega_A/dx$, and $\omega_A(x) = k_z V(x)$, the natural field line Alfvén frequency. In the present experiments, $k_z = \pi$. We employ a uniform grid in x, and the grid size in x is chosen to resolve the smallest $L_{ph}(x,t)$. However, this may result in inefficient gross overresolution where $L_{ph}(x,t)$ is greater than the minimum $L_{ph}(x,t)$. To avoid such inefficiency, the medium is chosen to have $L_{ph}(x,t)$ independent of x over most of the domain. This is achieved by a density profile producing the following Alfvén speed variation:

$$V(x) = (1 - \frac{x}{x_o}), \qquad 0 \le x \le x_c \tag{1}$$

and

$$V(x) = 1/\sqrt{a + bx + cx^2}, \qquad x_c < x \le 1 \tag{2}$$

Here we wish to excite two Alfvén resonances. This was achieved by setting $x_o = 1.0$ and $x_c = 0.8$ in our dimensionless units. From our previous considerations we also obtain $a = -575.0$, $b = 1250.0$, and $c = -625.0$. This results in an Alfvén speed that is 1 at $x = 0$ and falls linearly to 0.2 at $x = x_c$. Thereafter, $V(x)$ tails off less steeply to a minimum value of 0.1414 at $x = 1$. Since $V(x)$ is less steep in this latter range, $L_{ph}(x)$ is always greater than that in the linear portion; hence our grid spacing in x is still determined by the linear $V(x)$. The natural Alfvén waves resulting from this $V(x)$ have frequencies ranging from 3.142 at $x = 0$ to 0.445 at $x = 1$.

Following the analyses presented by *Walker et al.* [1992] and *Wright* [1994], we have produced the dispersion diagram for the first three fast eigenmodes shown in Figure 4. The conclusion of *Wright* [1994] (and confirmed in RW) is that the modes with small group velocities along the waveguide ($k_y \approx 0$ in this case) are the best drivers of resonances, since they have both a relatively coherent time dependence, and they do not propagate along the waveguide. For our chosen waveguide parameters we see that the $k_y \approx 0$ fast modes should drive resonances at $x \approx 0.24$ and $x \approx 0.564$, where the natural Alfvén waves ($\omega_A \approx 2.39$ and 1.37) have time periods of approximately 2.63 and 4.59, respectively. These are associated with the first two eigenmodes. However, the $n = 3$ eigenmode's frequency for $k_y = 0$ is ≈ 3.4, and hence lies outside the Alfvén continuum of our waveguide. (We have checked these WKB eigenfrequency estimates against a shooting method that can be used for $k_y = 0$ and find that we get agreement to within $\approx 3\%$.)

For future reference we also plot the group velocity along the waveguide V_g, say, against k_y for these eigenmodes in Figure 5, where $V_g = \partial\omega/\partial k_y$. The horizontal dashed line is the asymptotic group velocity (0.1414) to which all eigenmodes eventually tend in the limit of large k_y, i.e., $k_y/k_x \to \infty$ [see *Wright*, 1994].

For the initial perturbation we force u_x to satisfy $f(t)[1 + \cos(\pi y/\lambda_{yo})]/2$ at $x = 1$ for $0 \le t \le \tau$, where $0 \le y \le \lambda_{yo}$, $u_x(x = 1, y, t) = 0$ otherwise, and

$$f(t) = -[1 - \cos(4\pi t/\tau)]/2, \qquad 0 \le t < \tau/4$$

$$f(t) = -\sin(2\pi t/\tau), \qquad \tau/4 \le t \le 3\tau/4$$

$$f(t) = [1 - \cos(4\pi t/\tau)]/2, \qquad 3\tau/4 < t \le \tau$$

For the particular case of interest to us here we use $\tau = 2.35$ and $\lambda_{yo} = 0.2$ (which would scale to a distance of about $3R_E$ in the magnetosphere). The choice for $f(t)$ gives both u_x and $\partial u_x/\partial t$ zero at $t = 0$ and $t = \tau$. The boundary is imagined to start from rest. It is then pushed inward until $t = \tau/2$ and thereafter is returned to its original position at $x = 1$. The choice for τ was decided by the structure in y of the first two fast eigenmodes. The perturbations at $t = \tau$ produce significant overlaps with both of the eigenfunctions. Hence, in this case we anticipate that both eigenmodes will be significantly excited. This is motivated by Figure 1, which appears to show four relatively equally excited wave packets in b_ϕ.

Our numerical simulations run for a total time of $t = 40$. This allows significant time for the resonances

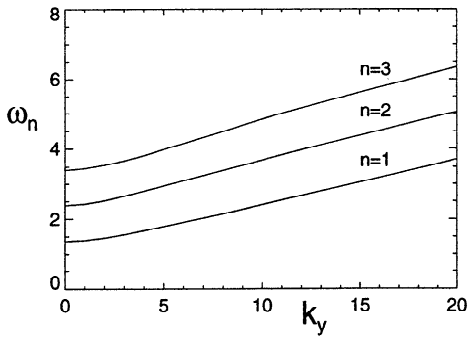

Figure 4. The fast mode dispersion diagram for the first three eigenmodes $n = 1$, $n = 2$, and $n = 3$ in the waveguide ($k_z = \pi$). The curves have been obtained from a WKB analysis. This results in small errors in the frequency estimates, particularly for $n = 2$, as opposed to frequencies obtained via a shooting method (see text).

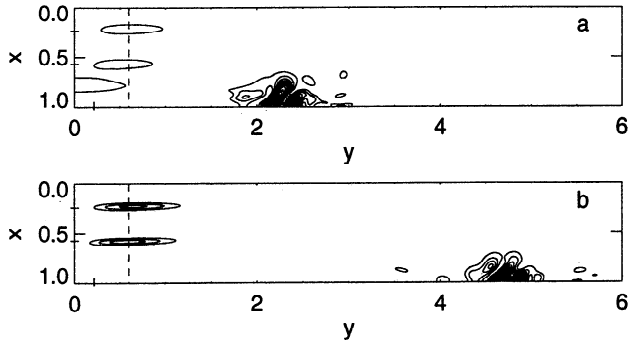

Figure 6. Contours of the total energy density at (a) $t = 20$ and (b) $t = 40$. The vertical dashed line is along $y = 0.6$. The horizontal dashes on the x axis ($y = 0$) mark the anticipated positions of the resonances. The vertical dash on the line $x = 1.0$ denotes the spatial extent in y of the initial perturbing pulse.

to develop. In Figure 6 we plot total energy density contours at $t = 20$ and $t = 40$. At $t = 20$ the maximum energy density is 8.795, while at $t = 40$ it is 8.274. We see that there are two significant features. The first is a pair of contours lying across the vertical dashed line at $y = 0.6$. At $t = 20$ these features are not so well defined, but by $t = 40$ they have grown in amplitude. In fact, between the two times the peak energy density in these features has approximately doubled from ≈ 0.6 to ≈ 1.2. As we shall see, these contours are due to the growth of the Alfvén resonances. The second significant feature lies farther down the waveguide. At $t = 20$ it lies between $y \sim 2$ and $y \sim 3$, and at $t = 40$ between $y \sim 4$ and $y \sim 5$. This is the fast mode energy which has not coupled to the resonances. The bulk of this energy is traveling at a speed of about 0.13. Inspection of Figure 5 reveals that this speed is a slight underestimate of the asymptotic group speed of 0.14 but gives us some confidence in our interpretation of this feature. An exact match would not in any case be expected since the fast mode dispersion and group velocity diagrams clearly show that both propagation and dispersion will be occurring, and therefore the energy density picture can only provide a relatively crude estimate in the first instance (see RW for a more detailed analysis of fast mode dispersion in a waveguide).

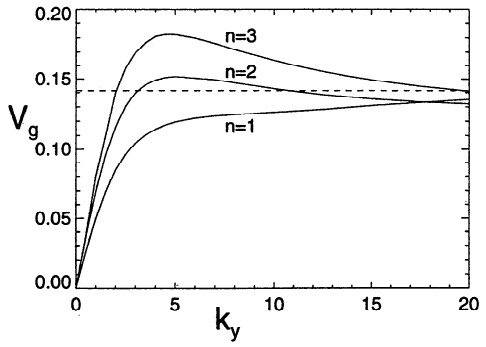

Figure 5. Group velocity V_g against k_y for the dispersion diagram in Figure 4. The horizontal dashed line denotes the asymptotic group velocity for large k_y.

The growth of the resonances is demonstrated in Figure 7, which shows snapshots of $b_y(x)$ along $y = 0.6$ at times $t = 10, 20$, and 40. We see the characteristic resonance development, i.e., phase mixing across the domain and preferential growth at specific locations. This justifies our assertion above that indeed the energy density contours straddling the line $y = 0.6$ are due to the resonances. As noted in RW, there is an approximate decoupling of the energy densities with either the fast modes or the Alfvén resonances. Any significant Alfvén resonances will be associated with structures in b_y; hence the plots shown in Figure 7. The vertical dashed lines mark the theoretically anticipated positions of the resonances (in good agreement with the results). We also see that the phase-mixing length at $t = 40$ is well resolved.

Figure 6 reconfirms the results of RW that indeed Alfvén waves with natural frequencies coincident with the $k_y \approx 0$ fast mode frequencies are excited. The predicted locations of the resonances found previously are marked on the x axis in Figure 6 with a horizontal dash, showing close correspondence with the development of significant energy density contours. The presence of more than one resonance does not appear to alter the thesis presented in RW. We also observe that the Alfvén waves that are excited lie close to the fast mode source as predicted by *Wright* [1994] (where the extent of the original perturbing source is marked with a vertical dash on the line $x = 1$).

Of all the possible satellite trajectories we could have chosen, let us consider the one shown in Figure 8. It is launched at $t = 10$ from the outer boundary $x = 1$ along $y = 0.5$. In the course of the simulation it traverses the width of the waveguide, arriving at $x = 0$ by $t = 40$. The timing and the location of this satellite have been chosen to allow it to pass through the expected sites of the resonances at times when they will have had sufficient time to develop into significant features. For the motives we outlined in section 2, such a satellite serves our purposes well and has a trajectory similar to that of DE 1 for the period of the data shown in Figure 1.

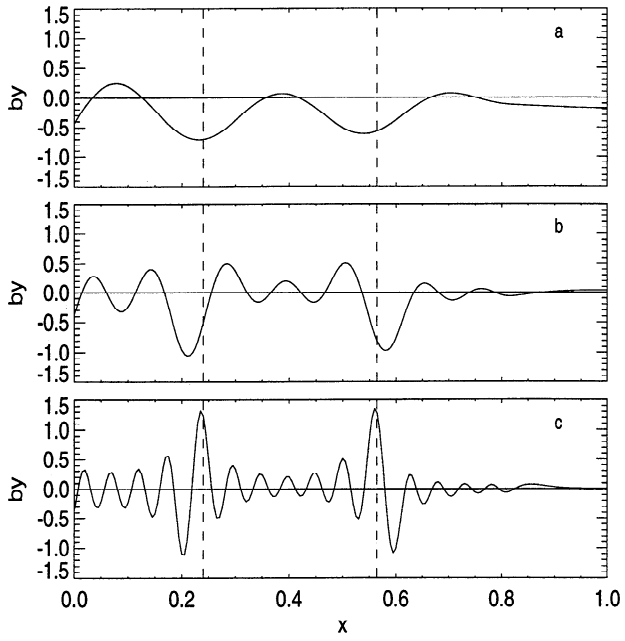

Figure 7. Profiles of b_y at $y = 0.6$ at times t of (a) 10, (b) 20, and (c) 40. The vertical dashed lines locate the expected positions of the resonances.

The major results are presented in Figure 9, which show the three magnetic field components sampled by the spacecraft as a function of time along its trajectory. For completeness the equivalent spacecraft locations "xsat" are also shown. Recalling the correspondence (b_z, b_x, b_y) to (b_μ, b_ν, b_ϕ) in Figure 1, we can make some immediate observations. First, the general characters of b_z and b_y match very well with b_μ and b_ϕ, respectively, apart from the interval 1600 UT to 1630 UT in b_ϕ. In particular, b_z exhibits the same characteristic decay in amplitude with time and also a reduction in period while never showing any evidence of smooth oscillations. Even more striking is b_y, with the wave packets associated with the resonances separated by low amplitude oscillatory signals quite evident (in our case two packets rather than four, of course). In further agreement with Figure 1, b_y is the main component in the pulsations over most of the observed interval.

It is clear from the data and the simulations that the Alfvén waves (b_y) are the dominant feature with respect to the fast modes (b_z) which are observed to decay away from the outer boundary. The relatively small amplitude of the fast mode (b_z) can be understood from the following points; (a) the fast mode is evanescent and thus not seen at small x; (b) as time increases the large k_y components of the fast mode propagate away from the satellite down the waveguide, and so are no longer observed; and (c) the small k_y components are of course responsible for driving the resonances, and hence their decay in amplitude is reflected in the growth of the Alfvén waves.

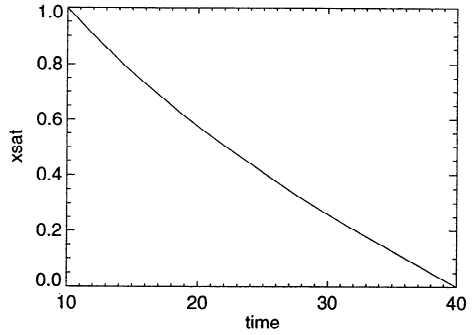

Figure 8. Trajectory in x (xsat) as a function of time for the satellite along $y = 0.5$.

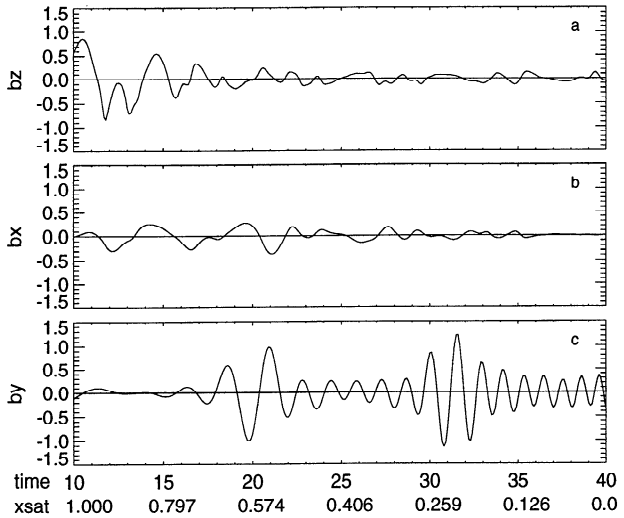

Figure 9. Magnetic fields (a) b_z, (b) b_x, and (c) b_y obtained from the satellite with trajectory shown in Figure 8. The horizontal axis is labelled by both the time and the equivalent satellite location xsat.

The present numerical experiment also confirms that resonances can indeed be generated by a spatially localized perturbation impinging on the outer boundary. *Lin et al.* [1992] do surmise that their pulsations result from a spatially localized source at the magnetopause, so this extra correspondence adds to the overall relevance of our results.

Although we find excellent correlation between many features in our simulations and real data, the agreement is not complete. In particular, the signatures from the interval 1600 UT to 1630 UT of Figure 1 are not evident in our results. The discrepancy may be attributable to our treating the magnetosphere as a cold plasma with a stationary magnetopause, whereas in reality we would expect a warm magnetosphere with a magnetopause capable of supporting surface waves.

5. Conclusions

We feel that through numerical experiments we have given some credence to the scenario put forward by *Lin et al.* [1992] to explain the magnetic pulsation data observed by the satellite DE 1. While we have only presented one possible satellite's eye view, it nevertheless corresponds very well in the overall features. There are clearly more detailed discrepencies (in particular, the nature of the data at times 1600 UT to 1630 UT).

However, the character of the pulsations themselves is well represented.

Our results also show that the apparent lack of any clear fast mode signatures is not at odds with the MHD waveguide view of the magnetosphere. The fast mode components either disperse and decay in amplitude as they propagate away from the souce region, or they find themselves converted into Alfvén waves close to where they were initially generated. On the basis of our results (see Figure 6 for example) the best way to observe the fast mode is to remain close to the magnetopause boundary and let the fast mode signature pass over you, rather than flying inward across the L shells to where the fast mode is evanescent. Indeed, RW give examples of such data (their Figure 7b). However, even this signal will decay in amplitude as it propagates and disperses. Moreover, the satellite will not observe a quasi-monochromatic b_z signal, confounding a straightforward search for waveguide modes. These properties are quite different to cavity modes, where a damped oscillatory fast mode is expected [*Lee and Lysak,* 1989]. The absence of fast mode signatures in data, which have a coherent oscillatory frequency and extend across a wide range of L shells, are in no way contradicted by the waveguide model (although it may suggest some inadequacies in the cavity model).

In conclusion, we feel that the MHD waveguide view of the Earth's magnetosphere is able to accurately predict many of the subtle features seen in the data and to explain apparent inconsistencies. We do not pretend that we have yet reached anything approaching realistic magnetospheric parameters. However, there is no reason yet to suppose that the generic properties that we detail will not be retained as the increases in computing power allow us to get closer to having a "working magnetosphere" on our desk.

Acknowledgments. This work was carried out while one of us (A.N.W.) was supported by a UK PPARC Advanced Fellowship. The authors are grateful to N. Lin for supplying the material in Figure 1 and to W. J. Hughes and M. J. Engebretson for useful discussions.

The Editor thanks O. W. Lennartsson and B. G. Harrold for their assistance in evaluating this paper.

References

Harrold, B. G., and J. C. Samson, Standing ULF modes of the magnetosphere: A theory, *Geophys. Res. Lett., 19,* 1811, 1992.

Hu, Y. Q., and S. T. Wu, A full-implicit-continuous-eulerian (FICE) scheme for multidimensional transient magnetohydrodynamic (MHD) flows, *J. Comput. Phys., 55,* 33, 1984.

Kivelson, M. G., and D. J. Southwood, Coupling of global magnetospheric MHD eigenmodes to field line resonances, *J. Geophys. Res., 91,* 4345, 1986.

Lee, D. H., and R. L. Lysak, Magnetospheric ULF wave coupling in the dipole model: The impulsive excitation, *J. Geophys. Res., 94,* 17,097, 1989.

Lin, N., M. J. Engebretson, L. A. Reinleitner, J. V. Olson, D. L. Gallagher, L. J. Cahill Jr., J. A. Slavin, and A. M. Persoon, Field and thermal plasma observations of ULF pulsations during a magnetically disturbed interval, *J. Geophys. Res., 97,* 14,859, 1992.

Rickard, G. J., and A. N. Wright, Alfvén resonance excitation and fast wave propagation in magnetospheric waveguides, *J. Geophys. Res., 99,* 13,455, 1994.

Samson, J. C., B. G. Harrold, J. M. Ruohoniemi, and A. D. M. Walker, Field line resonances associated with MHD waveguides in the magnetosphere, *Geophys. Res. Lett., 19,* 441, 1992.

Vanajakshi, T. C., K. W. Thompson, and D. C. Black, Boundary value problems in magnetohydrodynamics (and fluid dynamics), I, Radiation boundary condition, *J. Comput. Phys., 84,* 343, 1989.

Walker, A. D. M., J. M. Ruohoniemi, K. B. Baker, R. A. Greenwald, and J. C. Samson, Spatial and temporal behaviour of ULF pulsations observed by the Goose Bay HF radar, *J. Geophys. Res., 97,* 12,187, 1992.

Wright, A. N., Dispersion and wave coupling in inhomogeneous MHD waveguides, *J. Geophys. Res., 99,* 159, 1994.

G. J. Rickard and A. N. Wright, Department of Mathematical and Computational Sciences, University of St. Andrews, St. Andrews, Fife KY16 9SS, Scotland, U.K. (e-mail:grahamr@dcs.st-andrews.ac.uk; andy@dcs.st-andrews.ac.uk)

(Received September 7, 1994; revised November 9, 1994; accepted November 10, 1994.)